Electronic Supplementary Information (ESI)

Bright mechanoluminescent luminogen even in daylight through close intermolecular interaction with the characteristic of hybridized local and charge transfer (HLCT)

Dan Li,[a,d] Jie Yang,[a*] Yunsheng Wang,[a] Xiaoning Li,[a] Dongxia Zhu,[d*] Manman Fang,[a] Zhen Li[a,b,c*]

Table of Contents

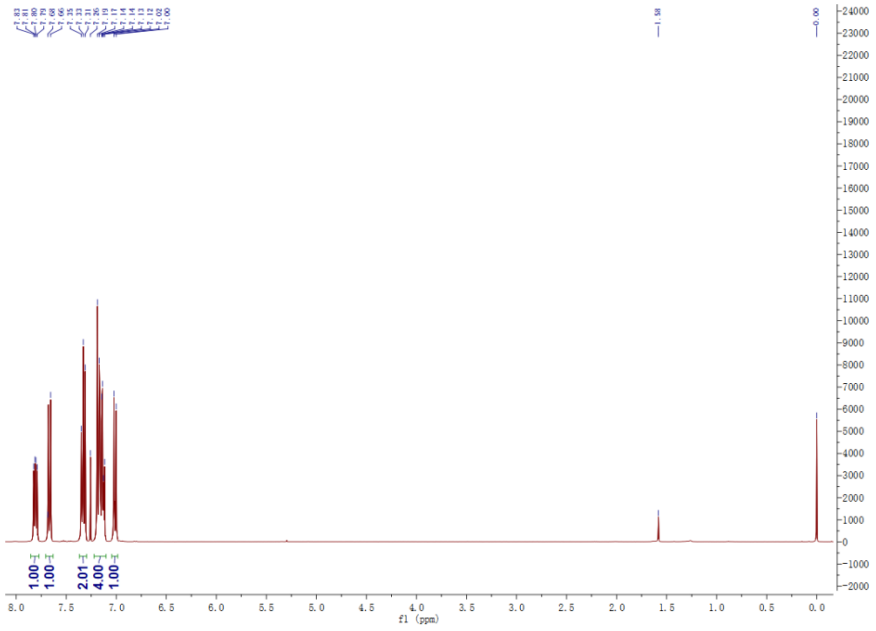

Figure S1. The ^{1}H NMR spectrum of FCO-TPA.

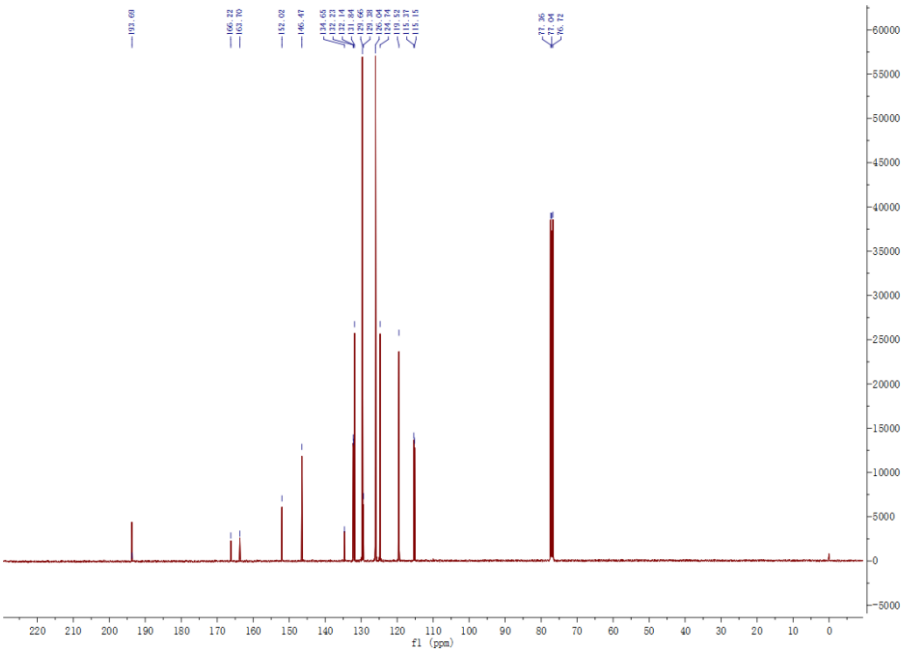

Figure S2. The ^{13}C NMR spectrum of FCO-TPA.

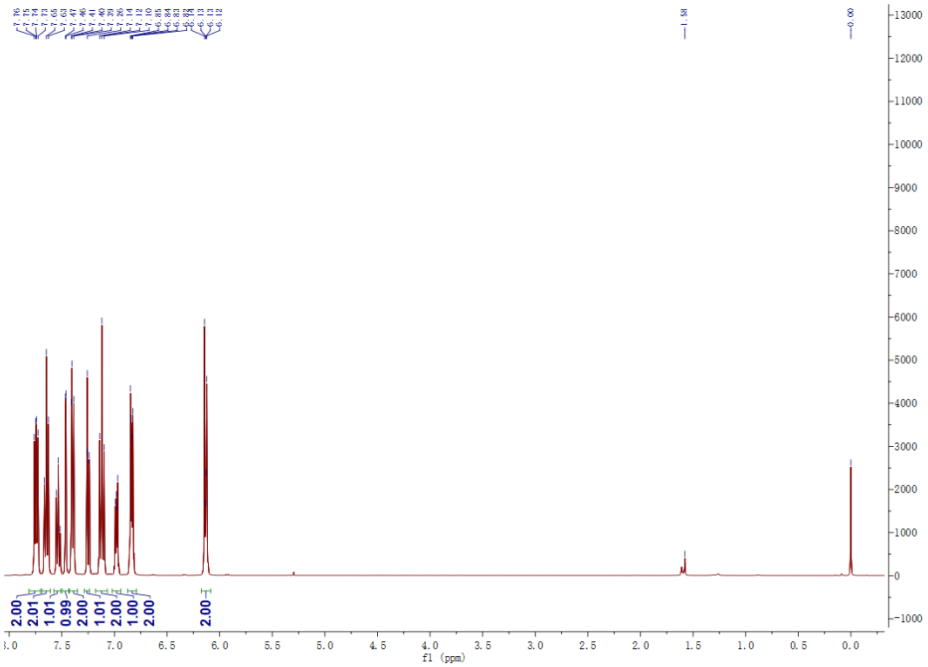

Figure S3. The ^{1}H NMR spectrum of FCO-CzS.

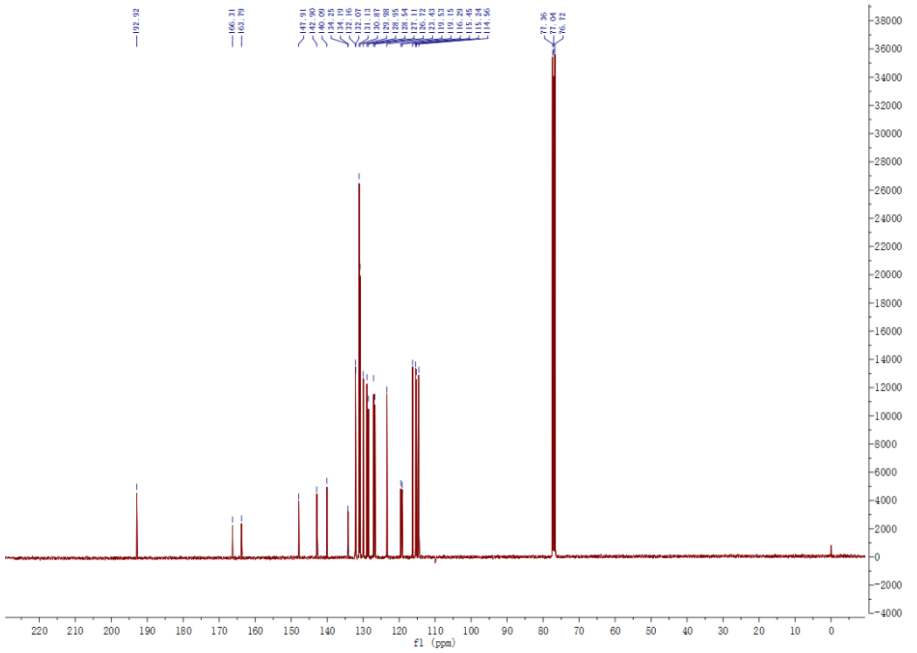

Figure S4. The ^{13}C NMR spectrum of FCO- CzS.

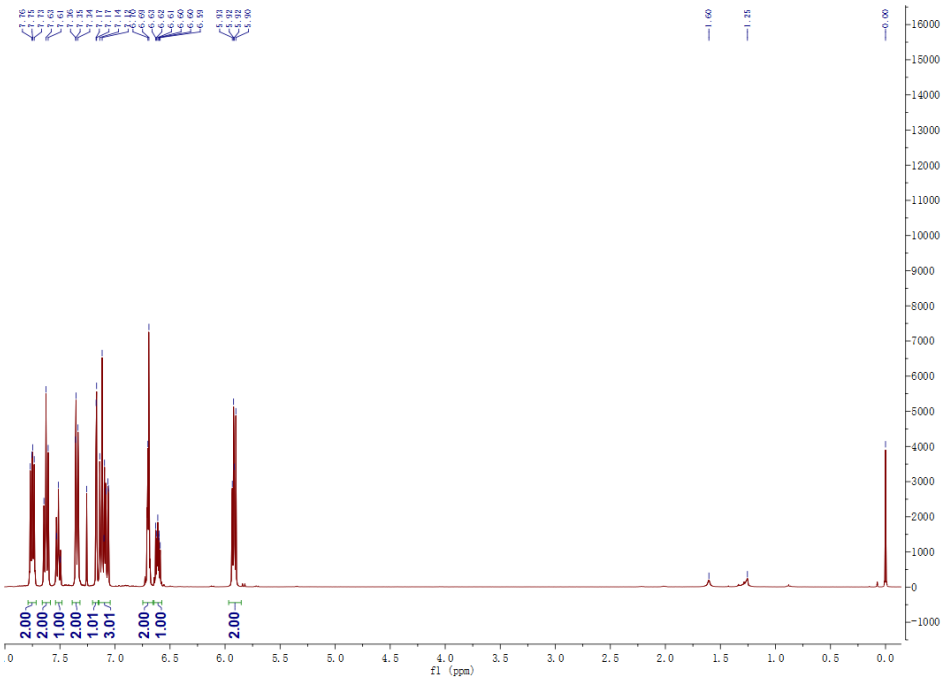

Figure S5. The ^{1}H NMR spectrum of FCO-CzO.

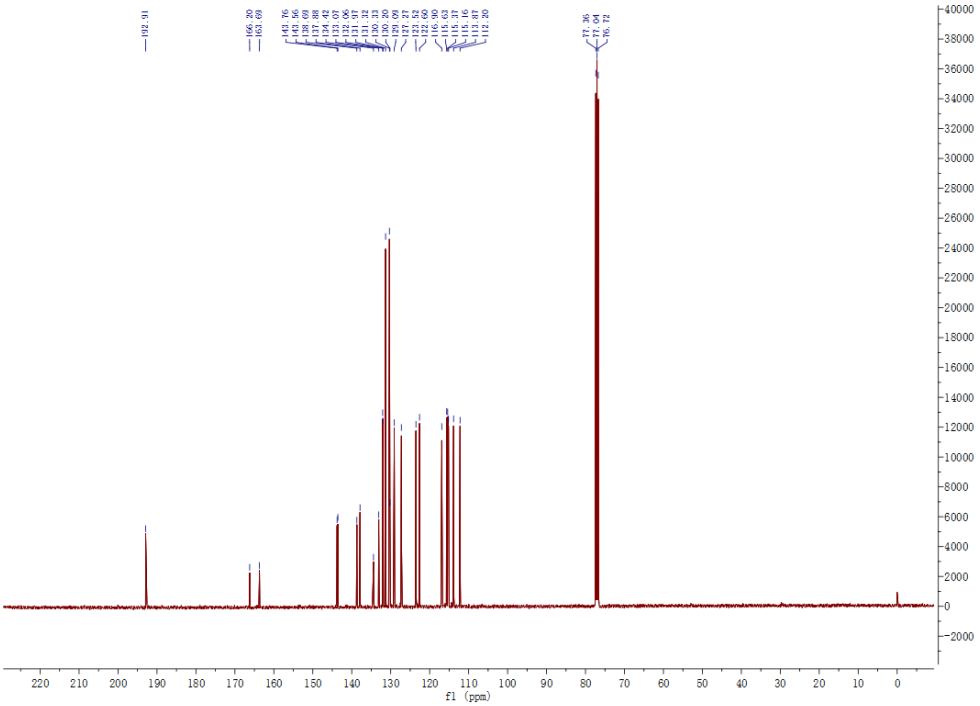

Figure S6. The ^{13}C NMR spectrum of FCO- CzO.

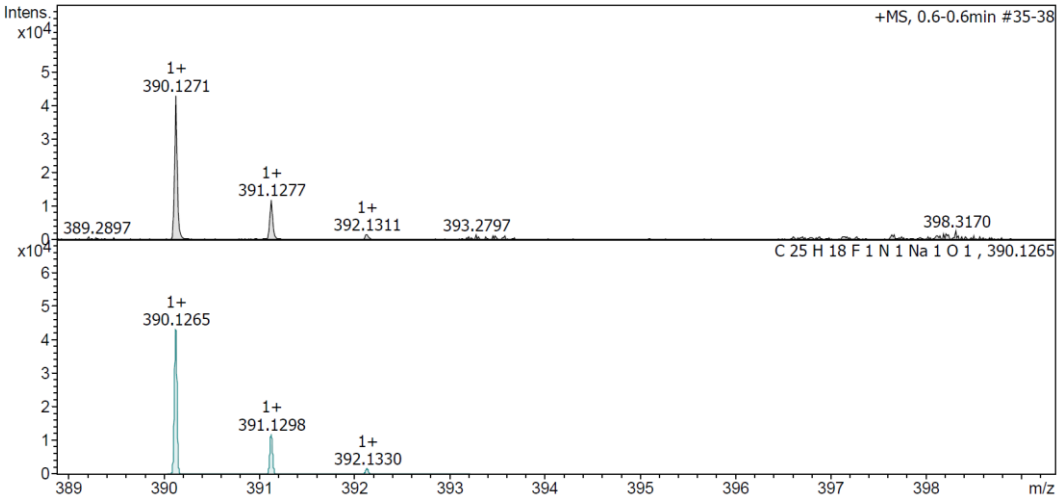

Figure S7. The high resolution mass spectrum of FCO-TPA.

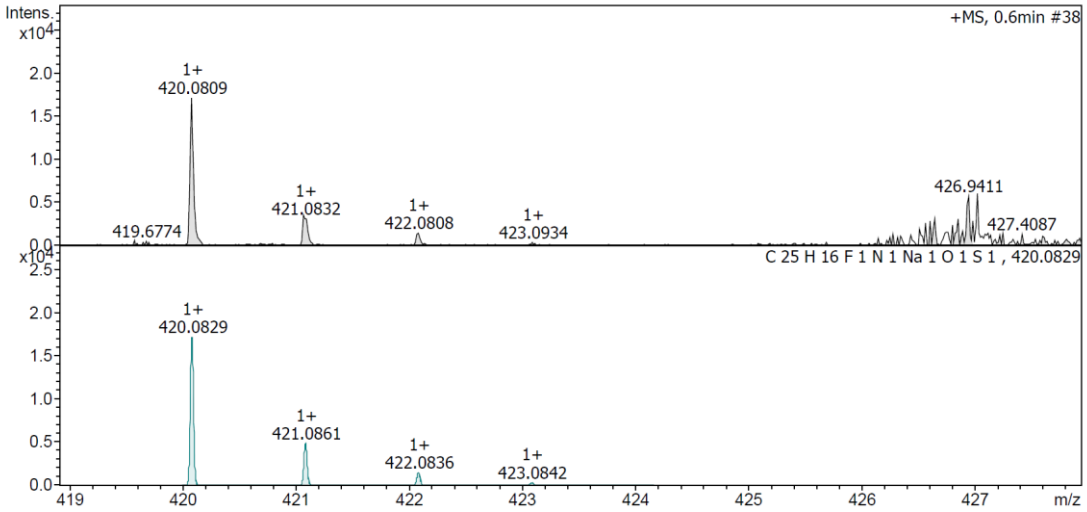

Figure S8. The high resolution mass spectrum of FCO-CzS.

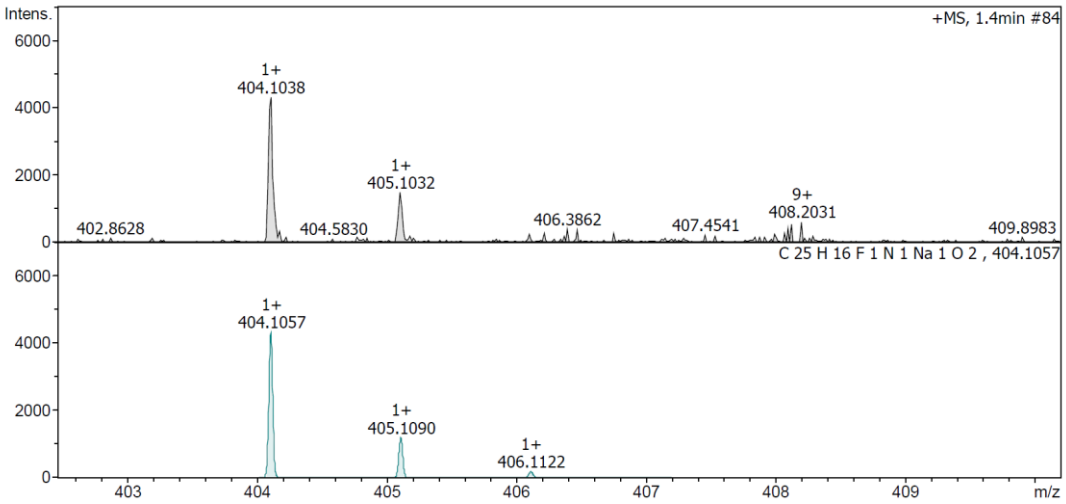

Figure S9. The high resolution mass spectrum of FCO-CzO.

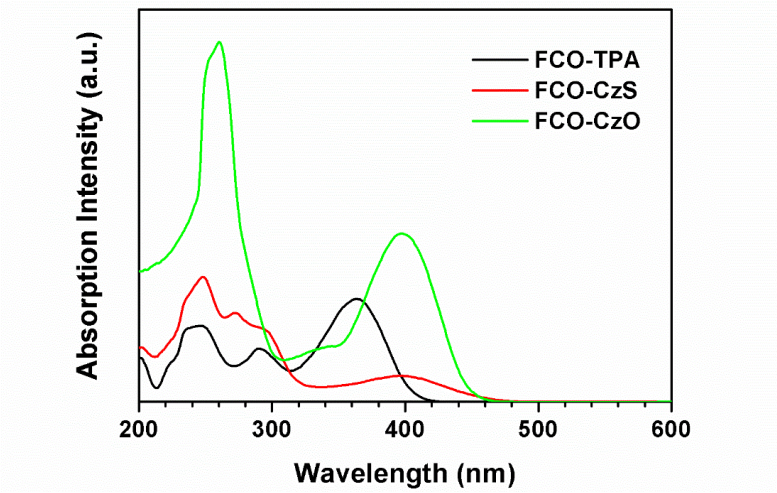

Figure S10. The UV-visible spectra of FCO-TPA, FCO-CzS and FCO-CzO in THF solution.

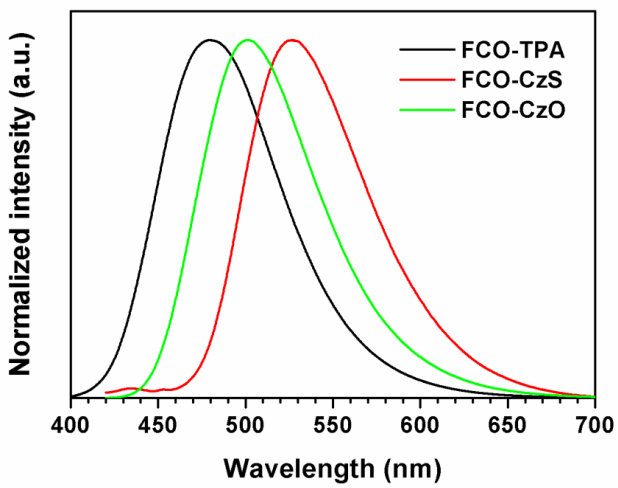

Figure S11. The emission spectra of FCO-TPA, FCO-CzS and FCO-CzO in THF solution.

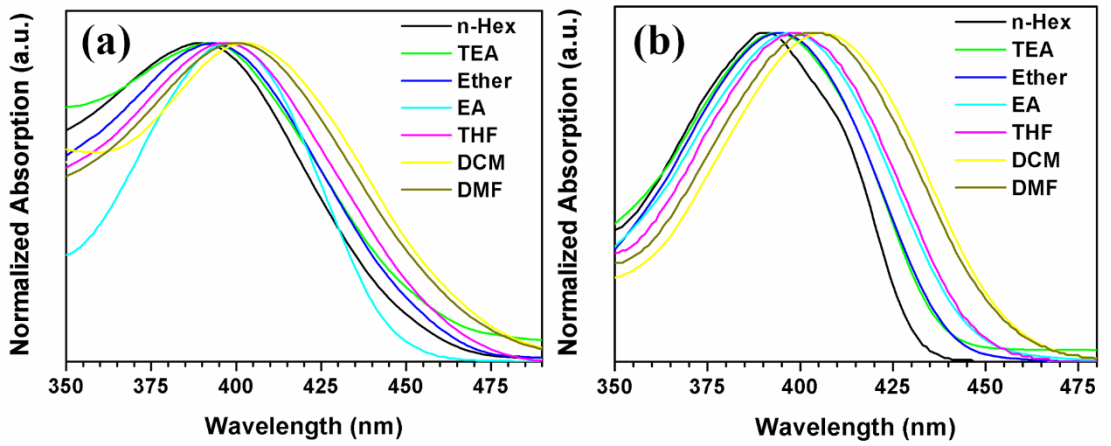

Figure S12. The UV-visible spectra of (a) FCO-CzS and (b) FCO-CzO in different solvents.

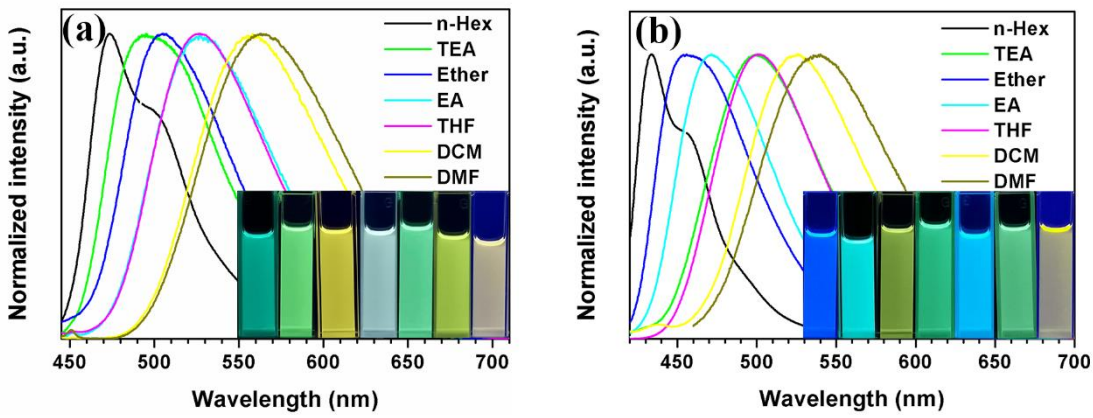

Figure S13. PL spectra of FCO-CzS and FCO-CzO in different solvents.

Solvatochromic effect

The influence of solvent environment on the optical property of our compounds can be understood using the Lippert-Mataga equation:

$$hc\ (v_a - v_f) = hc\ (v^0{}_a - v^0{}_f) + \frac{2\Delta\mu^2}{a^3} f(\varepsilon, n).$$

where $a = \sqrt[3]{\frac{3M}{4\pi d N_a}}$

In the above equations, v_a-v_f is the Stokes shift, , h is Planck's constant, c is the velocity of light, a is the Onsager radius of fluorophore, $\Delta\mu = \mu_e - \mu_g$ is the difference in the dipole moment of fluorophore between the excited (μ_e) and the ground (μ_g) states, e and n are the static dielectronic constant and the refractive index of the solvent, respectively, Δf is the orientation polarizability, M is the molecular weight, d is the density of molecule, and N_a is Avogadro's number. Therefore, based on equation, the change in dipole moment, $\Delta\mu = \mu_e - \mu_g$, can simply be estimated from the slope of a plot of v_a-v_f against Δf.

Table S1. Detailed absorption and emission peak positions of FCO-TPA, FCO-CzS and FCO-CzO in different solvents.

Solvents	ε	n	$f(\varepsilon,n)$	FCO-TPA			FCO-CzS			FCO-CzO		
				λ_a (nm)	λ_f (nm)	$\nu_a - \nu_f$ (cm^{-1})	λ_a (nm)	λ_f (nm)	$\nu_a - \nu_f$ (cm^{-1})	λ_a (nm)	λ_f (nm)	$\nu_a - \nu_f$ (cm^{-1})
Hexane	1.9	1.375	0.0012	357	410	3621	389	473	4565	390	434	2600
Triethylamine	2.42	1.401	0.048	360	432	4630	392	499	5470	394	456	3451
Ether	4.34	1.352	0.167	359	452	5731	393	505	5643	394	472	4194
Ethyl acetate	6.02	1.372	0.200	362	485	7006	397	527	6214	397	500	5189
Tetrahydrofuran	7.58	1.407	0.210	364	480	6639	397	526	6178	398	504	5166
Methylene dichloride	8.93	1.424	0.217	369	508	7415	402	557	6922	406	526	5619
N,N-dimethylformamide	37	1.427	0.276	365	526	8386	400	562	7206	403	540	6295

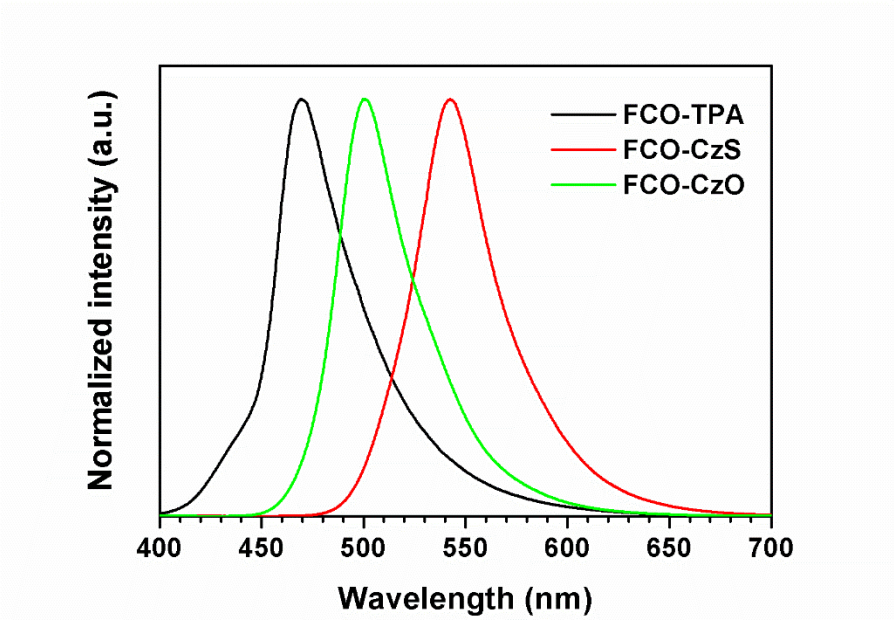

Figure S14. The emission spectra of FCO-TPA, FCO-CzS and FCO-CzO in solid state.

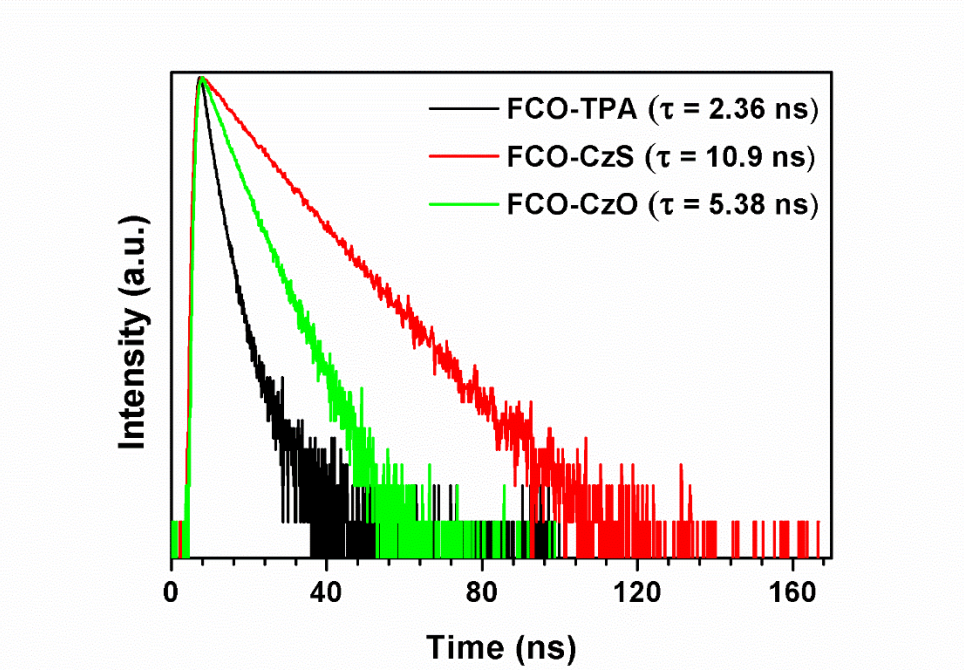

Figure S15. Emission decay curves of FCO-TPA, FCO-CzS and FCO-CzO in solid state.

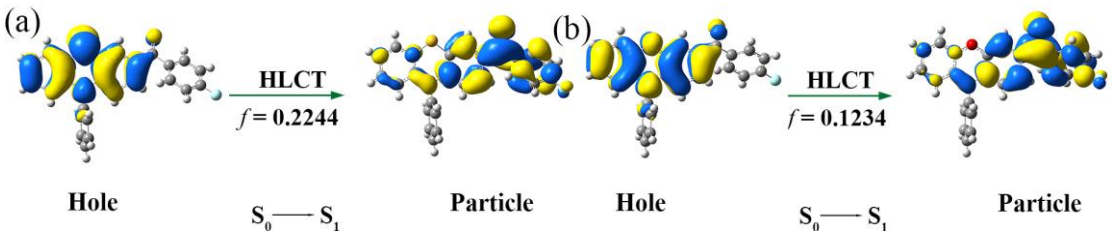

Figure S16. $S_0 \rightarrow S_1$ natural transition orbital (NTO) for FCO-CzS (a) and FCO-CzO (b).

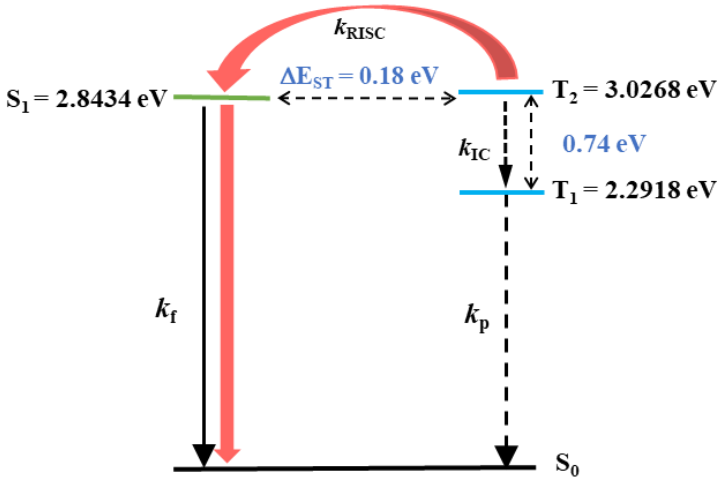

Figure S17. The simple model for exciton relaxation process and calculated singlet–triplet energy of FCO-CzS.

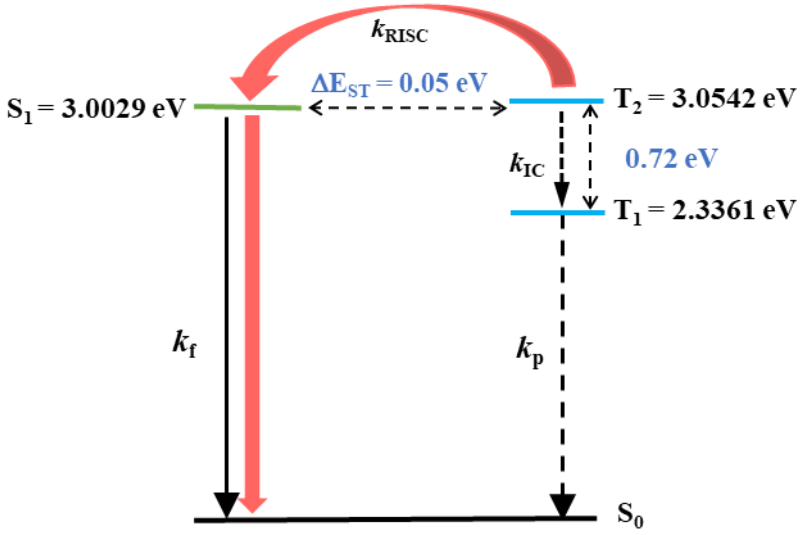

Figure S18. The simple model for exciton relaxation process and calculated singlet–triplet energy of FCO-CzO.

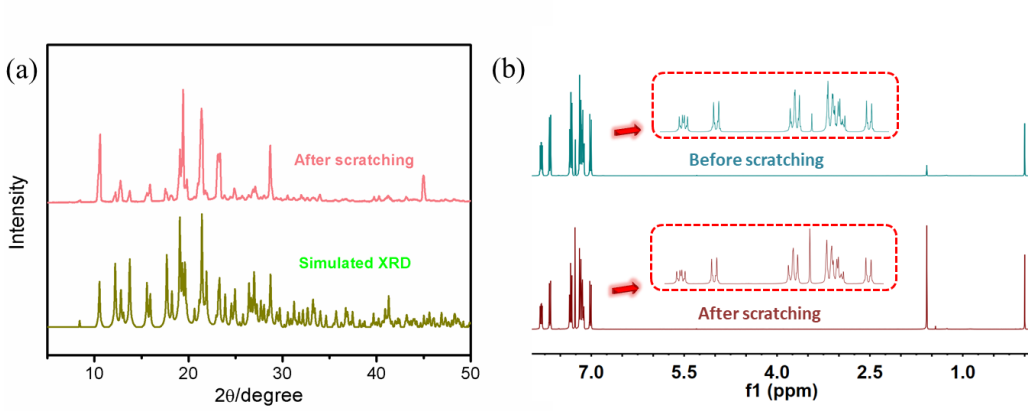

Figure S19. The (a) PXRD and (b) ^{1}H NMR of FCO-TPA before and after scratching.

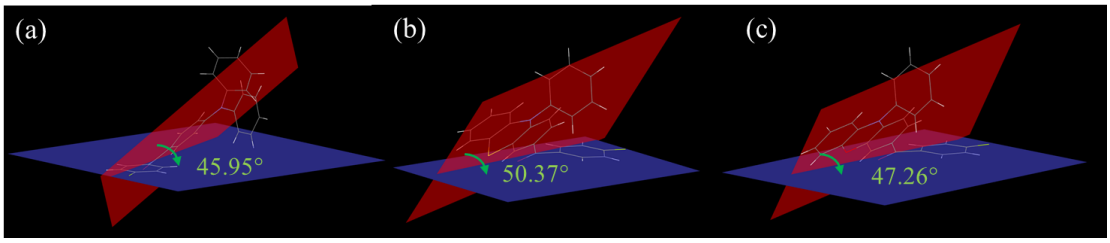

Figure S20. The D-A twist angles of (a) FCO-TPA (45.95°), (b) FCO-CzS (50.37°) and (c) FCO-CzO (47.26°).

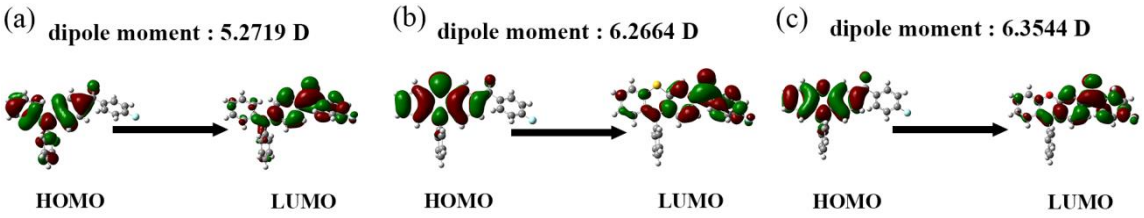

Figure S21. The HOMO/LUMO orbital distributions and dipole moments of the isolated molecules for FCO-TPA (a) FCO-CzS (b) and FCO-CzO (c).

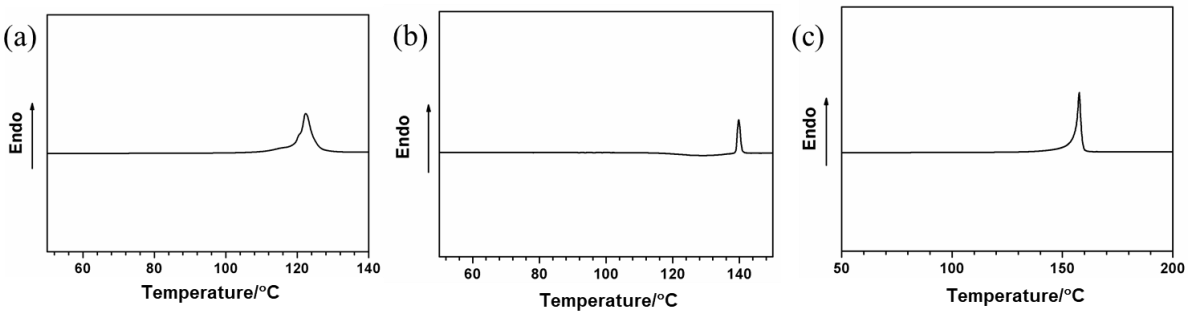

Figure S22. The DSC data of (a) FCO-TPA, (b) FCO-CzS and (c) FCO-CzO.

Table S2 Crystal data and structure refinement for FCO-TPA.

	1
Empirical formula	$C_{25}H_{18}FNO$
Formula weight	367.40
Temperature (K)	296
Crystal system	orthorhombic
space group	Pna21
a /Å	20.990(4)
b /Å	9.1680(16)
c /Å	10.0159(18)
α /°	90
β /°	90
γ /°	90
V/Å^3	1927.4(6)
Z	4
ρ_{calc}(g/cm^3)	1.266
μ/mm^{-1}	0.083
R_{int}	0.0351
Goodness-of-fit on F^2	1.044
R_1[a], wR_2[b] [I>2σ(I)]	0.0422,0.1029
R_1, wR_2 (all data)	0.0653,0.1149

[a] $R1 = \Sigma||Fo| - |Fc||/\Sigma|Fo|$. [b] $wR^2 = \{ \Sigma[w(Fo^2 - Fc^2)^2]/ \Sigma[w(Fo^2)^2]\}^{1/2}$

Table S3 Crystal data and structure refinement for FCO-CzS.

	1
Empirical formula	$C_{26}H_{16}F\ Cl_2NOs$
Formula weight	397.08
Temperature (K)	298
Crystal system	triclinic
space group	P-1
a /Å	9.1731(2)
b /Å	11.0168(3)
c /Å	111.6865(4)
α /°	115.261(3)
β /°	101.427(2)
γ /°	92.737(2)
V/Å^3	1035.18(5)
Z	2
ρ_{calc}(g/cm^3)	1.541
μ/mm^{-1}	4.013
R_{int}	0.0574
Goodness-of-fit on F^2	1.630
R_1[a], wR_2[b] [I>2σ(I)]	0.1029, 0.3289
R_1, wR_2 (all data)	0.1085, 0.3450

[a] $R1 = \Sigma||Fo| - |Fc||/\Sigma|Fo|$. [b] $wR^2 = \{ \Sigma[w(Fo^2 - Fc^2)^2]/ \Sigma[w(Fo^2)^2]\}^{1/2}$

Table S4 Crystal data and structure refinement for FCO-CzO.

	1
Empirical formula	$C_{25}H_{16}FNO_2$
Formula weight	381.39
Temperature (K)	298
Crystal system	triclinic
space group	P-1
a /Å	8.85361(17)
b /Å	9.38414(18)
c /Å	11.7086(2)
α /°	99.9418(16)
β /°	98.5741(16)
γ /°	94.0033(16)
V/Å^3	942.91(3)
Z	2
ρ_{calc}(g/cm^3)	1.343
μ/mm^{-1}	0.750
R_{int}	0.0256
Goodness-of-fit on F^2	1.057
R_1[a], wR_2[b] [I>2σ(I)]	0.0472,0.1174
R_1, wR_2 (all data)	0.0501,0.1214

[a] $R1 = \Sigma||Fo| - |Fc||/\Sigma|Fo|$. [b] $wR^2 = \{ \Sigma[w(Fo^2 - Fc^2)^2]/ \Sigma[w(Fo^2)^2]\}^{1/2}$